ACS APPLIED POLYMER MATERIALS

pubs.acs.org/acsapm Article

Comparison of High-Throughput and Conventional Tensile Testing for 3D-Printed Polymers

Daniyal Shoukat,[δ] Javaz T. Rolle,[δ] Jay Hoon Park, J. Carson Meredith,* and Nese Orbey*

Cite This: ACS Appl. Polym. Mater. 2024, 6, 9430−9439 Read Online

ACCESS | Metrics & More | Article Recommendations | Supporting Information

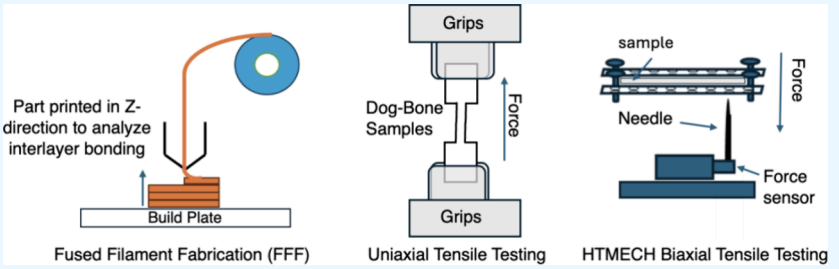

ABSTRACT: Fused filament fabrication (FFF) is a promising three-dimensional (3D) printing technology that is used to print prototypes for numerous applications. However, FFF printing results in poor interlayer bonding and inadequate mechanical performance of the printed parts, limitations that hinder its application for printing fully functional objects. Here, the tensile properties of FFF-printed samples were evaluated using various volume compositions of polycarbonate (PC)- and polycaprolactone (PCL)-based filaments under different print conditions. As conventional uniaxial tensile testing can be time-consuming, this study developed and analyzed the utility of a high-throughput mechanical analysis (HTMECH) method for rapidly screening the tensile properties and interlayer bonding of FFF-printed samples. The tensile properties obtained by uniaxial tensile testing of dog bones were compared to properties obtained by HTMECH testing of single-layer and bilayer films. Uniaxial tensile testing results for dog bones printed from filaments with a lower glass transition temperature (T_g) revealed that an increase in extrusion temperature and a decrease in layer thickness result in a higher tensile strength, owing to better interlayer bonding. When HTMECH was used, although single-layer films followed the same trends as dog bones, bilayer films showed an opposite trend, namely, tensile strength decreased as the extrusion temperature increased. Owing to a poor correlation between uniaxial tensile test results on dog bones vs HTMECH results on bilayer films, both methods were used to characterize the sample geometry of dog bones. Using either method, PC-based single-material and multimaterial dog bones showed an increase in tensile strength as extrusion temperature increased, a trend that was attributed to better interlayer bonding at higher temperatures. In conclusion, HTMECH is a useful method for rapidly screening the mechanical properties of 3D-printed samples affected by interlayer bonding by reducing the testing time compared to conventional uniaxial tensile testing methods.

KEYWORDS: *fused filament fabrication (FFF), interlayer bonding, uniaxial tensile testing, high-throughput mechanical analysis, polycarbonate, polycaprolactone*

1. INTRODUCTION

Additive manufacturing is the layer-by-layer formulation of a three-dimensional (3D) object, whereby a computer-aided design model is transformed into a physical product through successive layer stacking. Additive manufacturing is increasingly used in modern-day small-scale manufacturing facilities for prototyping, as well as in industrial-scale facilities for aerospace,[1−3] automotive,[4] and biomedical applications.[5−7] A key advantage lies in its ability to produce complex geometrical structures with minimal material waste.

One of the most commonly used rapid prototyping methods in additive manufacturing is fused filament fabrication (FFF). Owing to the efficient and cost-effective nature of the printing process, FFF has been widely applied in the biomedical,[8−10] pharmaceutical,[11,12] electronic,[13−15] and toy industries.[16,17] Yet FFF has not completely replaced traditional plastic manufacturing methods such as injection molding, which allows high-dimensional stability, smooth surface finish, and, importantly, enhanced mechanical performance.[18,19] The FFF printing process entails rapid heating and cooling cycles, which result in the formation of voids or pores that greatly reduce the strength of printed parts and contribute to poor interfacial

Received: March 25, 2024
Revised: June 3, 2024
Accepted: August 2, 2024
Published: August 7, 2024

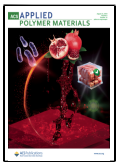

adhesion. Consequently, the FFF-printed parts exhibit anisotropic properties, with parts printed in the *Z*-orientation exhibiting up to 40−50% lower tensile strengths[20] than parts printed in the *XY*-plane.[21−24] FFF parts also suffer from other print defects, such as dimensional inconsistencies, thermal shrinkage, and residual stress build-up.[25]

Several studies have investigated the effects of different print conditions on the mechanical performance of FFF-printed parts. Coogan and Kazmer[26] found that higher extrusion temperatures result in improved tensile properties and stronger interlayer adhesion due to enhanced diffusion and chain entanglement across the layer interface. In a very similar study, Kuznetsov et al.[27] used a three-point bend test to evaluate the effect of extrusion temperature on the flexural strength of polylactic acid (PLA) parts printed in the *Z*-direction. They found that increased extrusion temperature results in improved flexural strength, which was attributed to an increase in material deposition and better interlayer adhesion. Liaw et al.[28] found extrusion temperature to be the most important print condition in enhancing the flexural strength of poly(ether ether ketone) (PEEK), owing to better interlayer adhesion. Fang et al.[29] determined the effect of nozzle temperature on polycarbonate (PC) printed parts. They observed that higher extrusion temperatures lead to better mechanical behavior and improved interlayer adhesion because the layers spend increased time above the glass transition temperature (T_g), resulting in higher tensile strength. Barile et al.[30] noticed that as extrusion temperature increased, the mechanical performance of the acrylonitrile butadiene styrene (ABS)-printed double cantilever beam samples improved, owing to better interlayer bonding.

Layer thickness has also been reported to affect tensile properties and interlayer adhesion significantly. Coogan and Kazmer[26] noted that a decrease in layer thickness leads to higher aspect ratios and greater contact area between successive layers, resulting in stronger interlayer bonds. Thinner layers require a higher deposition pressure, which results in better contact between layers, leading to a stronger interface and, hence, better mechanical properties.[26] Fang et al.[29] observed the same trend, finding that a reduction in layer thickness leads to a higher bond width and enhanced tensile strength. Pulipaka et al.[31] observed layer thickness to be one of the most important factors affecting the tensile strength of PEEK, with a lower layer thickness resulting in a higher tensile strength because of better interlayer bonding.

As a result, it is important to understand how composition, thermal and print conditions, and interlayer adhesion affect the mechanical properties of FFF-printed parts. Of relevance to this study, it is challenging to print dog-bone samples in the *Z*-direction for tensile testing, especially when using thermoplastics with a high T_g, such as PC. However, it is time-consuming to test mechanical properties using traditional uniaxial tensile methods according to ASTM. Therefore, the use of rapid testing methods that can quickly screen large "libraries" of samples and processing conditions would greatly accelerate screening of mechanical properties and interfacial adhesion.

High-throughput mechanical characterization (HTMECH) accelerates the screening of the mechanical (tensile) properties of polymers and their dependence on factors like composition and processing history.[32] HTMECH tools that miniaturize tensile testing have been developed to enable rapid collection of measurements (e.g., hundreds of data points per hour) of strength and other properties of film samples.[33] For example, the instrumented hemispherical indenter tool contacts films normal to the surface, extracting measurements of the modulus, tensile strength, and elongation at the break.[34] The instrument has been adapted to measure small values of adhesion between liquid-bridged surfaces,[35] so the question arises whether it could sensitively detect interlayer adhesion, in addition to tensile properties, in FFF-printed samples. However, no previously published report has described the use of HTMECH to characterize the 3D-printed samples.

The objective of this study was to develop high-throughput testing methods for screening the mechanical properties of FFF-printed parts utilizing HTMECH on printed single and bilayer films and to compare the results with mechanical properties obtained using conventional uniaxial tensile test methods. Different compositions of each of two different resins, PC and polycaprolactone (PCL), were used. The goal was to study the effects of the print condition and filament volume composition on the mechanical properties and to examine whether the mechanical properties and interlayer adhesion can be meaningfully determined via HTMECH measurements.

2. MATERIALS AND METHODS

2.1. Materials. Materials used in this work were selected from commercially available filaments; hence, commercially available PC filaments were selected because of their high T_g and PCL filaments were selected to print materials having a low T_g. PC and PCL filaments, each measuring 1.75 mm in diameter, were used. Two compositions of neat PC filaments were used: 90% PC (PolyLite) from Polymaker and 100% PC from Sigma-Aldrich. Polycarbonate filament reinforced with carbon fiber was also used: CF-PC (CarbonX eZPC + CF) from 3DXTECH. The CF-PC filament consists of 5−10 μm-wide carbon fibers making up 15% of the filament's composition. Two compositions of neat PCL filaments were used: 97% PCL (Facilan Ortho) and 100% PCL (Facilan PCL100), both from 3D4Makers.

90% PC and 97% PCL contain additives that make up the remaining composition of the filaments. These filaments are used in this study to analyze the effect of additives on material thermal and rheological properties and to evaluate the mechanical properties and interlayer bonding of 3D-printed samples compared to filaments with no additives.

2.2. Characterization. Filaments were characterized using differential scanning calorimetry (DSC) to determine and compare the T_g values of different compositions of PC and PCL, using a DSC2500 instrument (TA Instruments). Heat−cool−heat cycles were used to remove any processing history. For 90% PC and 100% PC and CF-PC filaments, the temperature was first increased to 270 °C at a rate of 10 °C/min; it was held at this temperature for 3 min, cooled to 25 °C at a rate of 5 °C/min, and then increased back to 270 °C at a rate of 10 °C/min. For 97 and 100% PCL filaments, the temperature was first increased to 150 °C at a rate of 10 °C/min; it was held at this temperature for 3 min, cooled to −90 °C at a rate of 5 °C/min, and then increased back to 150 °C at a rate of 10 °C/min. For both PC and PCL, T_g was determined from the change in the slope of the heat flow curve from the second heating cycle.

An ARES-G2 parallel-plate rheometer (TA Instruments) was used to measure the viscoelastic properties under oscillatory shear. The rheometer uses circular discs of 25 mm diameter for measurements. The microinjection molding from Xplore was used to mold the discs for the rheometer. PC filaments were first pelletized, predried overnight at 80 °C, and molded at a melt temperature of 250 °C, mold temperature of 110 °C, and pressure of 6 bar. PCL filaments were first pelletized and then molded at a melt temperature of 130 °C, mold temperature of 30 °C, and pressure of 6 bar. Molded discs were subsequently used in a parallel-plate rheometer.

https://doi.org/10.1021/acsapm.4c00921
ACS Appl. Polym. Mater. 2024, 6, 9430−9439

The linear viscoelastic region (LVR) was determined by carrying out a strain sweep from 0.1 to 100% at a 10 Hz frequency. A strain rate was selected from the region in which both moduli remained constant. A frequency sweep was carried out at this strain rate and a melt temperature of 250 °C for 90% PC and 100% PC and CF-PC and 130 °C for 97 and 100% PCL to obtain the complex viscosity.

2.3. FFF 3D Printing. *2.3.1. Single-Material Printing.* Creality Ender 5 Pro was used to print neat compositions of both materials (90% PC, 100% PC, 97% PCL, and 100% PCL) for single-material printing. However, the stock printer needed to be modified in several ways to allow efficient printing when using filaments with a high T_g, such as PC. First, the stock printer was equipped with a Bowden-type extruder, which was unable to apply sufficient pressure to the printed roads to lay down the correct road width. Therefore, the original extruder was replaced with a direct drive extruder (MicroSwiss) capable of providing sufficient pressure to the roads. The direct drive extruder was mounted directly above the nozzle. Second, the use of high temperatures necessary while printing filaments like PC can degrade the PTFE tubing in the stock hot end. Therefore, the stock hot end was replaced with an all-metal hot end (MicroSwiss) that allowed for high temperatures to be used while printing. Finally, to prevent rapid cooling of the layers and minimize thermal shrinkage and warpage of the printed parts, an acrylic enclosure (3DUPfitters) was used around the printer to control the convective heat transfer from the printed layers to the ambient atmosphere.

Three different types of samples were printed: (1) single-layer and bilayer films for HTMECH analysis, (2) dog-bone samples printed in the *Z*-direction for uniaxial tensile tests, and (3) rectangular samples printed in the *Z*-direction and subjected to waterjet cutting to obtain dog-bone samples for uniaxial tensile testing. A schematic representation showing the dimensions of dog bones obtained by direct printing or waterjet cutting of rectangular samples is shown in Figure S1. Print settings used during sample preparation are listed in Table 1. The effects of the extrusion temperature and layer thickness on the mechanical behavior were studied while keeping all other print conditions the same.

Table 1. Printing Conditions Used for Both Compositions of PC and PCL Filaments

print setting	90 and 100% PC	97 and 100% PCL
layer height	0.1 and 0.2 mm	0.2 mm
road width	0.5 mm	0.5 mm
infill percentage	100%	100%
raster angle	45°	45°
nozzle temperature	245, 250, and 255 °C	130 °C
bed temperature	110 °C	30 °C
print speed	20 mm/s	10 mm/s

2.3.2. Multimaterial Printing. FlashForge Creator 3 Pro was used to print CF-PC and 90% PC in a layer-by-layer fashion for multimaterial printing. The printer is equipped with direct drive-independent dual extruders, capable of printing two different materials simultaneously, and is fully enclosed, ensuring minimal heat loss to the surroundings during printing, requiring no modifications to the stock printer.

For multimaterial printing, only one type of sample was prepared: rectangular samples printed in the *Z*-direction using alternate layers of CF-PC and 90% PC were subjected to waterjet cutting to obtain dog-bone samples for both uniaxial tensile testing and HTMECH analysis. This was done by using the same geometry (dog bones) for uniaxial tensile tests and HTEMCH analysis. The print settings used during multimaterial printing for both CF-PC and 90% PC are shown in Table 2. Along with multimaterial rectangular samples, 90% PC and CF-PC single-material rectangular samples were also printed using the same print conditions and subjected to waterjet cutting to obtain dog bones. The goal was to compare the tensile properties of multimaterial dog-bone samples with the single-material dog-bone samples. The effect of extrusion temperature was studied on the mechanical behavior of single-material and multimaterial samples while keeping all other print conditions the same.

Table 2. Printing Conditions Used for CF-PC and 90% PC Single-Material and Multimaterial Samples

print setting	CF-PC and 90% PC
layer height	0.2 mm
road width	0.5 mm
infill percentage	100%
raster angle	45°
nozzle temperature	250 and 260 °C
bed temperature	110 °C
print speed	40 mm/s

During multimaterial printing, while one of the extruders is printing a layer, the second extruder is idle while still heated up. This results in drooling of the filament from the idle extruder, which can lead to excess material being deposited on the rectangular sample during printing. To remove this excess material from the nozzle before a layer is printed, a wiping tower is printed that wipes off the drooling material from the nozzle. Lopes et al.[36] used the same method during multimaterial printing. The wiping tower is also printed to prepare single-material rectangular samples to ensure consistent print settings between single-material and multimaterial printing.

2.4. Mechanical Testing Using Conventional Uniaxial Tensile Testing Methods. *2.4.1. Uniaxial Tensile Testing on Samples Prepared Using a Single Material.* For all neat materials (90% PC, 100% PC, 97% PCL, and 100% PCL), tensile testing was performed on an Instron 5966 at a strain rate of 1 mm/min. Tensile bars were printed with neat PC according to ASTM D 638.[37] Type V specimens, 4 mm thick, were printed in the *Z*-direction according to the dimensions specified in Figure S1 and print conditions reported in Table 1.

For PC, due to its very high T_g, printing dog bones directly in the *Z*-direction resulted in defects, especially in the narrow section, while printing overhangs. The defects might act as stress concentrators, resulting in premature sample failure. To eliminate defects, rectangular samples (63.5 × 20 × 4 mm) were printed in the *Z*-direction, and then type V specimens were obtained by waterjet cutting. The tensile properties of the waterjet-cut and directly printed dog-bone samples were measured and compared.

For PCL, due to its low T_g, the dog-bone samples could not be directly printed in the *Z*-direction because it took too long for the PCL layers to solidify. Specifically, the previous PCL layer was still in a molten state when the next layer was deposited, which resulted in the deformation of the narrow section of the dog bone. Therefore, all dog bones for 97 and 100% PCL were obtained using waterjet cutting from 3D-printed rectangular samples (63.5 × 20 × 4 mm).

2.4.2. Uniaxial Tensile Testing on Multimaterial Samples. A multimaterial dog bone consisting alternate layers of two different materials cannot be printed directly as the curvature in the dog bone cannot be designed in a layer-by-layer fashion. Hence, all multi-material dog bones were obtained using waterjet cutting from 3D-printed rectangular samples (63.5 × 40 × 1 mm). ASTM D 638 type V[37] geometry was modified by increasing the overall width and narrow section's width two times while keeping the length of the specimen the same (63.5 mm). 90% PC and CF-PC single-material dog bones with modified geometry were also obtained using waterjet cutting of rectangular samples to compare the mechanical behavior with multimaterial dog bones. For all single-material and multi-material dog bones having modified dimensions, tensile testing was performed on an Instron 68SC-05 with pneumatic grips at a strain rate of 0.25 mm/min and a pressure of 6 bar.

2.5. Fracture Surface Analysis. After tensile testing, the fractured surface of the dog-bone samples was imaged by using a Zeiss Auriga scanning electron microscope (SEM). The samples were first gold sputter-coated using a Leica SCD500 sputter coater for 150 s and subsequently imaged under SEM at an accelerating voltage of 5 keV and a working distance of 11 mm.

https://doi.org/10.1021/acsapm.4c00921
ACS Appl. Polym. Mater. 2024, 6, 9430−9439

2.6. Mechanical Testing Using HTMECH. A custom-made HTMECH instrument[34,38] was used to assess the mechanical properties of the 3D-printed films prepared using neat PC and PCL filaments and single-material and multimaterial dog bones prepared using 90% PC and CF-PC. In HTMECH, free-standing films that were held firmly around a circular perimeter were deformed normal to the film plane by using a smooth, hemispherical probe attached to a force sensor, which made contact with the film over a small area in the film's center. The custom-built apparatus was described in prior publications.[33,34,38] This arrangement was a miniaturized version of the ASTM E 2546 instrumented indented probe test.[39] The force versus time were measured as the film was both bent and stretched at a constant velocity. For the hole geometry used in our study, the mechanical theory of shells was generally applied when the thickness was <1000 μm, which encompassed the range of samples examined here. The theory of membranes treats the case where bending stresses can be assumed to be negligible compared to in-plane stresses, due to the relative thickness and hole size. The in-plane stresses consisted of both radial and azimuthal components within the film. This geometry and its interpretation through analytical and numerical models have been discussed at length in the literature; see, for example, Wan and Liao.[40] In-plane force was calculated by use of knowledge of indentation depth (velocity × time) and hole radius to calculate a film angle in order to convert the detected normal force to an in-plane component. Stress was calculated from this in-plane force by dividing by the initial area at which the film was supported around its rim, 2π (radius) (initial thickness). Indentation depth was calculated by using the time recorded by the computer's clock and deformation speed, which was set to constant velocity of 10 mm/s. The strain was calculated by converting the normal strain to a radial actual deformation and dividing by the initial film radius (the hole radius). The ultimate tensile strength was denoted as the highest stress experienced in the stress−strain curve.

2.7. Sample Preparation for HTMECH Using FFF.

2.7.1. HTMECH Analysis on Films Prepared Using a Single Material. FFF was used to 3D-print single-layer and bilayer films using neat compositions of PC and PCL, at 245 and 250 °C for PC or at 130 °C for PCL. HTMECH was used to determine the tensile properties of the films. Obtained trends were compared with uniaxial tensile test results. Sample dimensions used to print single-layer and bilayer films were 50.8 × 50.8 mm. For single-layer films, the layer thickness was 0.2 mm. For bilayer films, the total thickness of the film was 0.2 mm with a single-layer thickness of 0.1 mm. All other print conditions were kept the same, as shown in Table 1.

2.7.2. HTMECH Analysis on Multimaterial Dog-Bone Samples. For multimaterial printing, dog bones with modified geometry were obtained using waterjet cutting. As HTMECH can test only very thin samples, the thickness of the dog bones was kept at 1 mm. Both single-material and multimaterial dog bones were tested using HTMECH. The obtained trends were compared with uniaxial tensile test results on dog bones.

3. RESULTS AND DISCUSSION

3.1. Characterization of Filaments. Filaments were characterized for their thermal and rheological properties. As shown in Figure S2, the presence of additives significantly lowered the T_g of 90% PC (112 °C) compared to 100% PC (144 °C), whereas only a slight difference was observed in the T_g of CF-PC (111 °C) compared to 90% PC. PCL filaments showed a semicrystalline behavior with no difference in T_g between the 97 and 100% PCL filaments (both −63 °C). The objective of conducting thermal characterization using DSC was to study the effect of additives on the material T_g (90% PC vs 100% PC and 97% PCL vs 100% PCL) and to determine if differences in T_g can be correlated to the tensile properties and interlayer bonding of 3D-printed samples. A material with a lower T_g is expected to have a higher tensile strength and better interlayer bonding compared to a material with a higher T_g printed at the same nozzle temperature. This is because the increased time that each layer spends above T_g before solidifying provides more time for polymer diffusion and chain entanglement to occur.

For rheological characterization, a strain rate of 2% was observed to be within the LVR. Hence, this strain rate was selected for the frequency sweep tests for all materials to obtain the complex viscosity. As shown in Figure S3, 100% PC had a higher viscosity than both 90% PC and CF-PC, and 100% PCL had a higher viscosity than 97% PCL.

The 90% PC and CF-PC had very similar T_g and viscosity values (see Figures S2 and S3, respectively) and, therefore, were selected for multimaterial printing.

3.2. Tensile Testing on FFF-Printed Dog Bones Using ASTM Uniaxial Tests and Single-Layer and Bilayer Films Using HTMECH. The goal of this work was to develop HTMECH as a rapid screening method to determine the tensile properties of the FFF-printed samples. The tensile properties of the FFF-printed dog-bone samples were measured by traditional ASTM uniaxial tensile tests, and these results were correlated to HTMECH-determined tensile properties of single-layer and bilayer films.

Although neat PC dog bones could be printed directly in the *Z*-direction, printing the narrow section was a challenge because of the very high T_g of PC (112−144 °C by DSC). Conversely, PCL dog bones could not be printed directly because of the very low T_g of PCL (−63 °C by DSC). Therefore, to obtain PCL dog-bone samples, waterjet cutting of rectangular samples printed in the *Z*-direction was used. Researchers have used this method previously to obtain dog bones from rectangular samples.[41,42] Another advantage is that printing rectangular samples also allows more uniform PC dog bones to be obtained.

As PC dog bones could be printed directly, we first determined whether waterjet cutting had any effect on the tensile properties. This was achieved by comparing the tensile strengths of dog bones printed directly vs those obtained using waterjet cutting (all printed using a 0.2 mm layer thickness). Figure 1 shows the results obtained for 90% PC at different extrusion temperatures.

At extrusion temperatures of 245 and 250 °C, waterjet-cut dog bones exhibited slightly higher tensile strength values than those printed directly. However, this difference was not

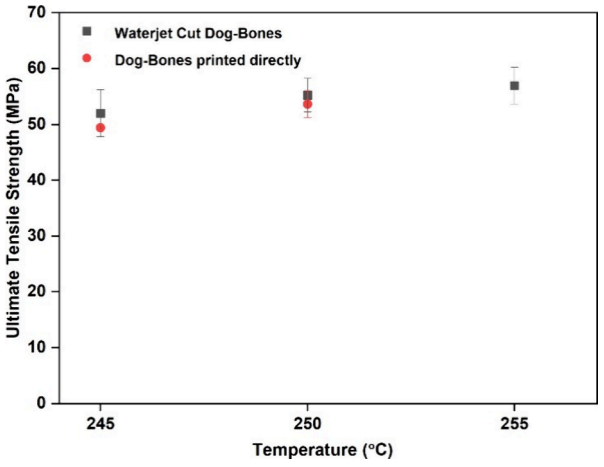

Figure 1. Tensile properties of 90% PC dog bones obtained by waterjet cutting vs direct printing, with a 0.2 mm layer thickness.

https://doi.org/10.1021/acsapm.4c00921
ACS Appl. Polym. Mater. 2024, 6, 9430−9439

statistically significant given the intrinsically high standard deviation of the tensile strength of FFF-printed samples. Therefore, it was concluded that the waterjet cutting of rectangular samples did not significantly alter the mechanical behavior of dog bones.

Figure 2 shows SEM images (×150 magnification) of the fractured surfaces of dog bones, obtained by direct printing or

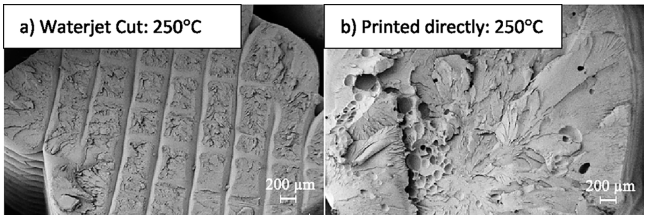

Figure 2. SEM images of 90% PC dog bones printed using a 0.2 mm layer thickness and 250 °C nozzle temperature obtained by (a) waterjet cutting and (b) direct printing.

waterjet cutting, printed at 250 °C using a 0.2 mm layer thickness. Similar observations were obtained at 245 and 255 °C, and the SEM images for all temperatures studied are shown in Figure S7 in the Supporting Information. Waterjet cutting resulted in samples with a very uniform interface with no voids, especially at 250 and 255 °C. Within each layer, infill lines printed at a 45° raster angle can be seen clearly. This uniformity arose because each layer had sufficient time to allow roads within each layer to completely solidify and bond before the deposition of the next layer, limiting void formation. Direct printing at either temperature resulted in samples with some voids because roads within each layer did not have sufficient time to solidify and bond completely before the next layer was deposited. Consequently, in the case of direct printing, infill lines cannot be seen in each layer.

Overall, no significant difference in mechanical behavior was observed between waterjet-cut and directly printed dog bones. This observation can be explained as follows. In the dog-bone samples obtained from waterjet cutting of rectangular samples, although each layer had more time for roads to bond completely before the next layer was deposited, the longer time allowed layers to cool, resulting in poor interlayer bonding. Conversely, in directly printed samples, although voids were present and acted as stress concentrators during tensile testing, the mechanical strength was only slightly lower than it was in waterjet-cut dog bones. The layers of the directly printed dog bones bonded more strongly to each other because each layer had less time to cool before the next layer was deposited, owing to the smaller dimensions of a dog bone compared to those of a rectangular sample. Hence, the higher interfacial temperature of the directly printed dog bones allowed increased polymer diffusion, leading to stronger interlayer bonding. Whereas rectangular samples showed comparatively poor interlayer bonding, directly printed dog bones exhibited voids. As a result, both sample types had similar tensile strengths. It is also important to note that a higher interfacial temperature might have caused the roads to fuse while still in a molten state, resulting in interfaces with indistinguishable infill lines. For all of these reasons, we decided that waterjet cutting to obtain PCL dog bones was a good approach.

3.2.1. Tensile Properties of 90% PC. The effect of three extrusion temperatures (245, 250, and 255 °C) on the mechanical performance of 90% PC was examined (Figure 1). As expected, an increase in extrusion temperature led to improvement in the tensile strength of directly printed and waterjet-cut dog bones. Similar results were reported previously.[26−29] At higher extrusion temperatures, the layers remained above T_g for longer before solidifying, allowing for better chain entanglement and better diffusion across layers, leading to enhanced interlayer adhesion. However, no significant change in tensile strength was observed beyond 250 °C. Fang et al.[29] observed the same trend, noting that diffusion and chain entanglement reached equilibrium after 250 °C, causing no further improvement in interlayer bonding. Therefore, the tensile properties of dog bones printed directly were evaluated only at 245 and 250 °C.

Next, the effect on the mechanical behavior of two-layer thicknesses (0.1 and 0.2 mm) of directly printed dog-bone samples was evaluated (Figure 3a). At 245 °C, the average

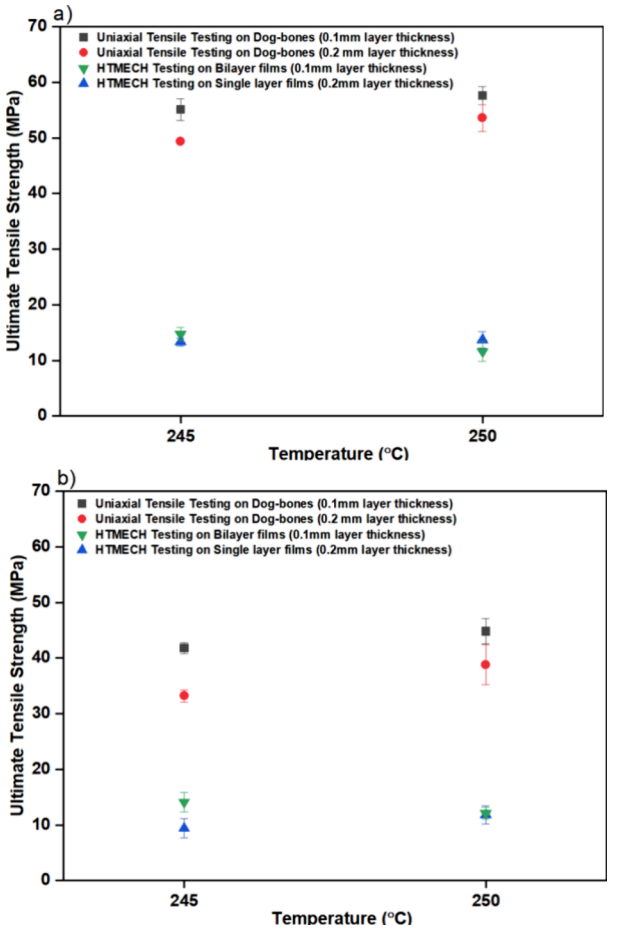

Figure 3. Tensile strength obtained using uniaxial tensile testing on dog bones printed directly and using HTMECH on single-layer and bilayer films of (a) 90% PC and (b) 100% PC.

tensile strength was 55.1 vs 49.4 MPa for dog bones printed with a layer thickness of 0.1 vs 0.2 mm, respectively. At 250 °C, the average tensile strength was 57.6 vs 53.6 MPa for dog bones obtained at a layer thickness of 0.1 vs 0.2 mm, respectively. Thus, a thinner layer thickness (0.1 mm) resulted in higher tensile strength, because the larger aspect ratio and increased contact area between the successive layers[26−29] enabled better interlayer bonding.

https://doi.org/10.1021/acsapm.4c00921
ACS Appl. Polym. Mater. 2024, 6, 9430−9439

SEM images of fractured surfaces at 0.1 mm layer thickness were obtained (Figure S8) and compared to fractured surfaces at 0.2 mm layer thickness. Comparison of Figure S7 with Figure S8 revealed some voids in both cases due to insufficient cooling, which resulted in poorer bonding of roads within each layer. A smoother cut was observed with the 0.1 mm layer thickness, which can be explained by the higher mechanical properties and better interlayer bonding resulting from the higher pressure required to deposit thinner layers.[26]

Films were printed using FFF, and mechanical properties were evaluated using HTMECH. Single-layer films (0.2 mm) and bilayer films (each layer 0.1 mm and total thickness of 0.2 mm) were printed at 245 and 250 °C while keeping all other printer parameters the same. Rather than seeking to obtain quantitative agreement between the HTMECH (film) and conventional uniaxial tensile testing (dog bone) results, the goal of this analysis was to detect similar trends with both methods. Results obtained with HTMECH are shown in Figure 3a. As expected, the quantitative values of mechanical properties by HTMECH were smaller than those obtained by uniaxial tensile testing because the two testing methods used distinct modes of fracture. In a conventional ASTM tensile test, dog-bone samples underwent a uniaxial mode of fracture. In HTMECH, the films underwent a biaxial mode of fracture, in which stress and strain were distributed in multiple dimensions, resulting in lower overall stress (see Sormana et al.[34] for details). Crystal structure can also affect the results obtained from uniaxial and HTMECH testing. However, in this study, we did not study the effect of crystallinity because PC is an amorphous material. It can be observed from Figure 3a that an increase in the extrusion temperature led to an improvement in the tensile strength of single-layer films. However, for bilayer films, a decrease in tensile strength was observed, which contrasts the trend obtained using dog bones where an increase in extruder temperature led to a higher tensile strength attributed to better interlayer bonding. Hence, no correspondence was obtained between uniaxial tensile tests on dog bones and HTMECH tests on bilayer films, whereas for single-layer films, HTMECH results followed the same trend as the uniaxial tensile tests on dog bones.

In contrast to the original hypothesis, HTMECH results also demonstrated that there was no significant difference in the single-layer and bilayer results for the samples printed at 245 °C, while for the samples printed at 250 °C, there was only a small difference, where the single-layer film was slightly stronger. To test if HTMECH can detect a difference in the tensile strength of a bilayer film as the first layer is allowed to cool, we examined whether a wait time between layer depositions would influence the tensile strength by decreasing the interlayer adhesion. Bilayer films were printed with a wait time of 10 or 20 min between the deposition of the first and second layers. As shown in Table 3, there was no significant difference in the tensile strength of the bilayer films prepared with wait times of 10 or 20 min compared to those printed without any wait time.

3.2.2. 100% PC. A composition of 100% PC was used to print dog bones directly and to obtain rectangular samples for waterjet cutting using a 0.2 mm layer thickness. The 100% PC composition has a higher T_g than 90% PC and, thus, experiences greater thermal shrinkage and greater residual stress build-up. At an extrusion temperature of 245 °C, waterjet cutting of the 100% PC rectangular samples resulted in samples with very low tensile strength and a high standard deviation. Printing dog bones directly resulted in more consistent tensile properties. Hence, directly printed samples were selected to study the effect of print conditions on the mechanical performance of 100% PC. Two extrusion temperatures (245 and 250 °C) and layer thicknesses (0.1 and 0.2 mm) were used to directly print dog bones in the *Z*-direction. The results are shown in Figure 3b.

Table 3. Tensile Strength of 90 and 100% PC Single-Layer and Bilayer Films Obtained by HTMECH

	tensile strength (MPa) of 90% PC		tensile strength (MPa) of 100% PC	
single vs bilayer film, wait time	245 °C	250 °C	245 °C	250 °C
single layer	13.3 ± 0.7	14.7 ± 1.3	9.4 ± 1.7	11.8 ± 1.6
bilayer, no wait time	13.7 ± 1.5	11.6 ± 1.8	14.1 ± 1.7	12.1 ± 1.1
bilayer, 10 min wait time	14.0 ± 2.1	14.1 ± 2.3	9.3 ± 0.8	11.5 ± 1.1
bilayer, 20 min wait time	15.2 ± 1.1	14.4 ± 2.5	9.9 ± 0.5	11.9 ± 0.9

In both the 100 and 90% PC dog-bone samples, an increase in extrusion temperature and a decrease in layer thickness led to an increase in tensile strength owing to better interlayer bonding. However, the 100% PC samples showed a lower tensile strength than the 90% PC samples under all printing conditions. The presence of additives in the 90% PC samples resulted in a lower T_g (as shown by DSC), allowing more time for bond formation between subsequent layers and, thus, higher tensile strength. Compared with the 100% PC samples, the 90% PC samples had lower viscosity, which resulted in greater material deposition at the same extrusion temperature, formation of fewer voids, and higher tensile strength. The SEM images of the fractured surfaces of 100% PC (Figure S9) revealed a very porous interface, with larger and numerous pores compared to 90% PC. Samples printed at the 0.2 mm layer thickness had more pores than those printed at the 0.1 mm layer thickness, which explains the lower tensile strength obtained when using a larger layer thickness. At the 0.1 mm thickness, increased pressure resulted in deposition of a thinner layer that led to better contact between subsequent layers,[31] minimizing void formation.

Figure 3b shows the HTMECH results on single-layer and bilayer films. Like 90% PC, 100% PC single layers showed an improvement in the tensile strength as the extrusion temperature was increased. Moreover, 90% PC single-layer films were observed to have a higher tensile strength than 100% PC single-layer films at both extrusion temperatures as was also observed with uniaxial tensile tests on dog bones. However, in contrast to the case of 90% PC, bilayer films had higher-tensile-strength values than single-layer films for 100% PC, which suggested that interlayer bonding is affecting the mechanical properties of 90% PC and 100% PC differently. 100% PC bilayer films were printed with a wait time of 10 or 20 min between the deposition of the first and second layers (as was done with the 90% PC samples). Results are shown in Table 3. Unlike the 90% PC samples, the 100% PC bilayer films showed lower tensile strength measurements when a wait time of 10 min was used. No additional effect was observed with a 20 min wait time. In 100% PC that had a higher T_g than 90% PC, longer wait times that allowed cooling during deposition led to poorer interlayer adhesion, likely resulting from poor interlayer chain diffusion.

https://doi.org/10.1021/acsapm.4c00921
ACS Appl. Polym. Mater. 2024, 6, 9430−9439

3.2.3. 97 and 100% PCL. For both PCL filament compositions, rectangular samples were printed in the *Z*-direction and subsequently cut using waterjet. An extrusion temperature of 130 °C and a layer thickness of 0.2 mm were used. Uniaxial tensile testing results are shown in Table 4. No

Table 4. Tensile Strength of 97% PCL and 100% PCL Obtained Using Uniaxial Tensile Testing on Waterjet-Cut Dog Bones and HTMECH on Single-Layer and Bilayer Films

single or bilayer film, wait time	tensile strength (MPa) of 97% PCL	tensile strength (MPa) of 100% PCL
uniaxial tensile testing on dog bones	19.6 ± 1.4	20.3 ± 2.4
HTMECH testing on single-layer films	5.9 ± 1.1	5.0 ± 0.5
HTMECH testing on bilayer films, no wait time	6.1 ± 0.4	5.8 ± 0.5
HTMECH testing on bilayer films, 10 min wait time	6.6 ± 0.2	4.5 ± 0.5
HTMECH testing on bilayer films, 20 min wait time	5.6 ± 0.2	4.4 ± 0.8

significant difference was observed in the tensile strength between 97% PCL and 100% PCL. This result can be explained by the very similar thermal and rheological properties of both compositions, as measured by DSC and a parallel-plate rheometer, respectively. As the 97 and 100% PCL compositions were not significantly different in T_g or viscosity, no difference in interlayer bonding was expected when using the same print conditions. Since only one temperature was used to print PCL samples, the effect of crystallinity was not studied in this work.

Table 4 shows HTMECH results on single-layer and bilayer films for both 97% PCL and 100% PCL. Single-layer (0.2 mm) and bilayer (each layer 0.1 mm and total thickness of 0.2 mm) films were printed at 130 °C keeping the other printer parameters the same. HTMECH results for 97 and 100% PCL were very similar. The average tensile strength of the bilayer PCL films was higher than that of the single-layer PCL films. Table 4 shows the effect of the wait time on the tensile strength of bilayers. The 97 and 100% PCL compositions exhibited decreased tensile strength after 20 or 10 min, respectively. As with the 90% PC composition, the presence of additives in the 97% PCL composition helped to preserve interfacial adhesion during the wait time.

3.3. Tensile Testing on FFF-Printed Dog Bones Using ASTM Uniaxial Tests and HTMECH. In contrast to the original hypothesis, poor correspondence was obtained between uniaxial tensile tests on dog bones and HTMECH tests on bilayer films, where the bilayer films did not show an improvement in the tensile strength as the temperature was increased. In addition, different trends were obtained between the tensile strength of single-layer and bilayer films when using either 90% PC or 100% PC. Therefore, it was decided to move away from the film geometry for HTMECH tensile testing toward using dog bones for both uniaxial tensile tests and HTMECH analysis. Since HTMECH can test only very thin samples, the thickness of the dog bones was reduced to 1 mm. Testing 1 mm thick type V dog bones using uniaxial tensile testing, however, resulted in stress concentration within the grips, causing the dog bones to fracture in the grips. Hence, the type V geometry was modified by increasing the overall width and width of the narrow section twice while keeping the length the same (Figure S1b). This allowed the fracture to occur in the narrow section of the dog bone during uniaxial tensile testing.

Both 90% PC and CF-PC were used to print 1 mm thick single-material and multimaterial rectangular samples that were subjected to waterjet cutting to obtain dog bones. Since the width of the dog bones was increased, the width of the rectangular samples was also increased by two times (40 mm). Two different extrusion temperatures, 250 and 260 °C, were used to evaluate the mechanical performance of single-material and multimaterial samples. A layer thickness of 0.2 mm was used to prepare the samples at both extrusion temperatures. The results obtained using uniaxial tensile tests and HTMECH are shown in Figure 4. Using uniaxial tensile testing, the tensile

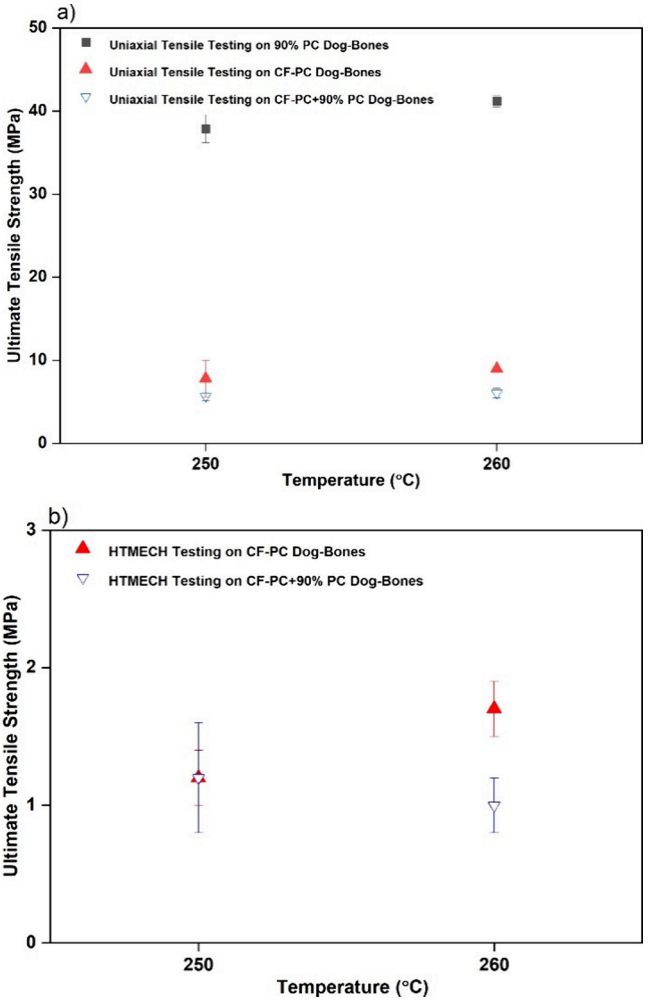

Figure 4. Tensile test results on 90% PC and CF-PC single-material and multimaterial dog bones using (a) uniaxial tensile testing and (b) HTMECH.

strength of 90% PC was observed to increase, while only a slight increase was observed for CF-PC single-material dog bones, which was attributed to better interlayer bonding. For multimaterial CF-PC + 90% PC dog bones, however, no statistical difference in tensile strength was observed at the two extrusion temperatures. This is because during dual-extrusion printing, a wiping tower is printed, which allows each extruder to wipe off the drooling material before printing a layer, causing the layers on the rectangular sample to cool before the

https://doi.org/10.1021/acsapm.4c00921
ACS Appl. Polym. Mater. 2024, 6, 9430−9439

next layer is deposited. Hence, no change in interlayer bonding is expected as the temperature is increased, resulting in a similar tensile strength at both extrusion temperatures. It is important to note that the wiping tower is also printed while printing 90% PC and CF-PC single-material rectangular samples. However, during single-material printing, the extruders do not need to be changed before printing each layer on the rectangular sample and the wiping tower, which results in less cooling time compared to that in a dual-extrusion print. Therefore, the tensile strength of 90% PC and CF-PC single-material dog bones is observed to improve as the extruder temperature is increased.

HTMECH results on the single-material and multimaterial dog bones are shown in Figure 4b. Because of the high tensile strength of the 90% PC dog bones, it could not be tested with HTMECH at both extrusion temperatures. Similar to uniaxial tensile testing, the tensile strength of CF-PC was observed to improve slightly as the extrusion temperature was increased, whereas no statistical difference was observed in the tensile strength of CF-PC + 90% PC dog bones at the two extrusion temperatures. Hence, as is evident from Figure 4, both uniaxial tensile testing and HTMECH resulted in the same trends whereby an improvement in tensile strength was observed as the extrusion temperature was increased.

4. CONCLUSIONS

This study used HTMECH as a rapid screening method to determine the tensile properties of FFF-printed samples as a function of the 3D-printing condition and volume composition of filament. Consistent trends were observed between the results of uniaxial tensile tests on dog bones and HTMECH tests on single-layer films, with an increased extrusion temperature leading to improved tensile properties for both sample types. However, HTMECH tests on bilayer films showed trends differing from those of uniaxial tensile tests for both the 90% PC and 100% PC filament compositions. This finding suggests that HTMECH is not useful for evaluating the mechanical behavior of the bilayer films. The tensile properties of single-layer and bilayer films by HTMECH differed depending on the material T_g. At 245 °C, for instance, bilayer films had higher tensile strengths than single-layer films for 100% PC, whereas no significant difference was observed for 90% PC. HTMECH results showed that longer wait times, designed to create conditions for poor interlayer diffusion and thus poor adhesion, affect tensile strength. Consistently, bilayer films printed with filaments containing additives (90% PC and 97% PCL) tended to show a preserved tensile strength even during an extended wait period. Thus, HTMECH can detect differences in mechanical behavior resulting from changes in filament composition (and, thus, filament T_g), but only when extended wait times are used.

Because of a poor correlation obtained between uniaxial tensile tests on dog bones and HTMECH analysis on bilayer films, both testing methods were subsequently used to evaluate dog bones printed using 90% PC, CF-PC, and CF-PC + 90% PC. Similar trends were observed using both uniaxial tensile testing and HTMECH, where the tensile strength of CF-PC improved as the extrusion temperature was increased, while no statistical difference was observed for the multimaterial CF-PC + 90% PC dog bones. Using the dog-bone geometry, it was shown that HTMECH served as a useful rapid screening method for evaluating the mechanical properties of 3D-printed samples, where a change in tensile properties can be detected as a function of the printing conditions.

■ ASSOCIATED CONTENT

Data Availability Statement

The HTMECH results showing the raw force vs time data for PC- and PCL-based samples can be accessed from https://hdl.handle.net/1853/75386.

Supporting Information

The Supporting Information is available free of charge at https://pubs.acs.org/doi/10.1021/acsapm.4c00921.

Thermal and rheological properties of all materials measured using DSC and a parallel-plate rheometer, respectively; stress−strain curves obtained for 90% PC using uniaxial tensile tests and HTMECH; SEM images of the fractured surfaces of 90% PC and 100% PC dog bones (PDF)

■ AUTHOR INFORMATION

Corresponding Authors

J. Carson Meredith − *School of Chemical and Biomolecular Engineering, College of Engineering, Georgia Institute of Technology, Atlanta, Georgia 30332, United States;* orcid.org/0000-0003-2519-5003; Email: Carson.Meredith@chbe.gatech.edu

Nese Orbey − *Department of Chemical Engineering, Francis College of Engineering, University of Massachusetts Lowell, Lowell, Massachusetts 01854, United States;* orcid.org/0000-0003-3973-5736; Email: Nese_Orbey@uml.edu

Authors

Daniyal Shoukat − *Department of Chemical Engineering, Francis College of Engineering, University of Massachusetts Lowell, Lowell, Massachusetts 01854, United States*

Javaz T. Rolle − *School of Chemical and Biomolecular Engineering, College of Engineering, Georgia Institute of Technology, Atlanta, Georgia 30332, United States*

Jay Hoon Park − *Department of Plastics Engineering, Francis College of Engineering, University of Massachusetts Lowell, Lowell, Massachusetts 01854, United States;* orcid.org/0000-0002-0665-4684

Complete contact information is available at: https://pubs.acs.org/10.1021/acsapm.4c00921

Author Contributions

$^{\delta}$D.S. and J.T.R. contributed equally to the paper.

Notes

The authors declare no competing financial interest.

■ ACKNOWLEDGMENTS

This material is based upon work supported by the National Science Foundation under Award Numbers 1822141, 1822147, and 1822157 Phase I IUCRC: Center for Science of Heterogeneous Additive Printing of 3D Materials (SHAP3D) and the SHAP3D IUCRC Members. Any opinions, findings, and conclusions or recommendations expressed in this material are those of the authors and do not necessarily reflect the views of the National Science Foundation or SHAP3D members.

REFERENCES

(1) Karkun, M. S.; Dharmalinga, S. 3D Printing Technology in Aerospace Industry – A Review. *International Journal of Aviation, Aeronautics, and Aerospace* **2022**.

(2) Pant, M.; Pidge, P.; Nagdeve, L.; Kumar, H. A Review of Additive Manufacturing in Aerospace Application. *Revue des composites et des matériaux avancés* **2021**, *31* (2), 109–115.

(3) Guo, N.; Leu, M. C. Additive manufacturing: technology, applications and research needs. *Frontiers of Mechanical Engineering* **2013**, *8* (3), 215–243.

(4) Shahrubudin, N.; Lee, T. C.; Ramlan, R. An Overview on 3D Printing Technology: Technological, Materials, and Applications. *Procedia Manufacturing* **2019**, *35*, 1286–1296.

(5) Yan, Q.; Dong, H.; Su, J.; Han, J.; Song, B.; Wei, Q.; Shi, Y. A Review of 3D Printing Technology for Medical Applications. *Engineering* **2018**, *4* (5), 729–742.

(6) Aimar, A.; Palermo, A.; Innocenti, B. The Role of 3D Printing in Medical Applications: A State of the Art. *Journal of Healthcare Engineering* **2019**, *2019*, 1–10.

(7) Wang, Y.; Ahmed, A.; Azam, A.; Bing, D.; Shan, Z.; Zhang, Z.; Tariq, M. K.; Sultana, J.; Mushtaq, R. T.; Mehboob, A.; et al. Applications of additive manufacturing (AM) in sustainable energy generation and battle against COVID-19 pandemic: The knowledge evolution of 3D printing. *Journal of Manufacturing Systems* **2021**, *60*, 709–733.

(8) Wang, Y.; Müller, W.-D.; Rumjahn, A.; Schmidt, F.; Schwitalla, A. D. Mechanical properties of fused filament fabricated PEEK for biomedical applications depending on additive manufacturing parameters. *J. Mech. Behav. Biomed. Mater.* **2021**, *115*, No. 104250.

(9) Beatrice, C. A. G.; Shimomura, K. M. B.; Backes, E. H.; Harb, S. V.; Costa, L. C.; Passador, F. R.; Pessan, L. A. Engineering printable composites of poly (ε-polycaprolactone)/β-tricalcium phosphate for biomedical applications. *Polym. Compos.* **2021**, *42* (3), 1198–1213.

(10) Alam, F.; Varadarajan, K. M.; Koo, J. H.; Wardle, B. L.; Kumar, S. Additively Manufactured Polyetheretherketone (PEEK) with Carbon Nanostructure Reinforcement for Biomedical Structural Applications. *Adv. Eng. Mater.* **2020**, *22* (10), No. 2000483.

(11) Eleftheriadis, G. K.; Katsiotis, C. S.; Genina, N.; Boetker, J.; Rantanen, J.; Fatouros, D. G. Manufacturing of hybrid drug delivery systems by utilizing the fused filament fabrication (FFF) technology. *Expert Opinion on Drug Delivery* **2020**, *17* (8), 1063–1068.

(12) Prasad, E.; Islam, M. T.; Goodwin, D. J.; Megarry, A. J.; Halbert, G. W.; Florence, A. J.; Robertson, J. Development of a hot-melt extrusion (HME) process to produce drug loaded Affinisol 15LV filaments for fused filament fabrication (FFF) 3D printing. *Addit. Manuf.* **2019**, *29*, No. 100776.

(13) Flowers, P. F.; Reyes, C.; Ye, S.; Kim, M. J.; Wiley, B. J. 3D printing electronic components and circuits with conductive thermoplastic filament. *Additive Manufacturing* **2017**, *18*, 156–163.

(14) Barši Palmić, T.; Slavič, J.; Boltežar, M. Process Parameters for FFF 3D-Printed Conductors for Applications in Sensors. *Sensors* **2020**, *20* (16), 4542.

(15) Salo, T.; Halme, A.; Lahtinen, J.; Vanhala, J. Enhanced stretchable electronics made by fused-filament fabrication. *Flexible Printed Electron.* **2020**, *5* (4), No. 045001.

(16) León-Cabezas, M. A.; Martínez-García, A.; Varela-Gandía, F. J. Innovative functionalized monofilaments for 3D printing using fused deposition modeling for the toy industry. *Procedia Manufacturing* **2017**, *13*, 738–745.

(17) Singh, S.; Singh, G.; Prakash, C.; Ramakrishna, S. Current status and future directions of fused filament fabrication. *Journal of Manufacturing Processes* **2020**, *55*, 288–306.

(18) Ahn, S. H.; Montero, M.; Odell, D.; Roundy, S.; Wright, P. K. Anisotropic material properties of fused deposition modeling ABS. *Rapid Prototyping Journal* **2002**, *8* (4), 248–257.

(19) Koch, C.; Van Hulle, L.; Rudolph, N. Investigation of mechanical anisotropy of the fused filament fabrication process via customized tool path generation. *Additive Manufacturing* **2017**, *16*, 138–145.

(20) Gao, X.; Qi, S.; Kuang, X.; Su, Y.; Li, J.; Wang, D. Fused filament fabrication of polymer materials: A review of interlayer bond. *Addit. Manuf.* **2021**, *37*, No. 101658.

(21) Chacón, J. M.; Caminero, M. A.; García-Plaza, E.; Núñez, P. J. Additive manufacturing of PLA structures using fused deposition modelling: Effect of process parameters on mechanical properties and their optimal selection. *Materials & Design* **2017**, *124*, 143–157.

(22) Gonabadi, H.; Yadav, A.; Bull, S. J. The effect of processing parameters on the mechanical characteristics of PLA produced by a 3D FFF printer. *International Journal of Advanced Manufacturing Technology* **2020**, *111* (3–4), 695–709.

(23) Rodríguez-Panes, A.; Claver, J.; Camacho, A. The Influence of Manufacturing Parameters on the Mechanical Behaviour of PLA and ABS Pieces Manufactured by FDM: A Comparative Analysis. *Materials* **2018**, *11* (8), 1333.

(24) Ghorbani, J.; Koirala, P.; Shen, Y.-L.; Tehrani, M. Eliminating voids and reducing mechanical anisotropy in fused filament fabrication parts by adjusting the filament extrusion rate. *Journal of Manufacturing Processes* **2022**, *80*, 651–658.

(25) Yin, B.; He, Q.; Ye, L. Effects of deposition speed and extrusion temperature on fusion between filaments in single-layer polymer films printed with FFF. *Advanced Industrial and Engineering Polymer Research* **2021**, *4* (4), 270–276.

(26) Coogan, T. J.; Kazmer, D. O. Bond and part strength in fused deposition modeling. *Rapid Prototyping Journal* **2017**, *23* (2), 414–422.

(27) Kuznetsov, V. E.; Solonin, A. N.; Tavitov, A.; Urzhumtsev, O.; Vakulik, A. Increasing strength of FFF three-dimensional printed parts by influencing on temperature-related parameters of the process. *Rapid Prototyping Journal* **2020**, *26* (1), 107–121.

(28) Liaw, C.-Y.; Tolbert, J. W.; Chow, L. W.; Guvendiren, M. Interlayer bonding strength of 3D printed PEEK specimens. *Soft Matter* **2021**, *17* (18), 4775–4789.

(29) Fang, L.; Yan, Y.; Agarwal, O.; Seppala, J. E.; Hemker, K. J.; Kang, S. H. Processing-structure-property relationships of bisphenol-A-polycarbonate samples prepared by fused filament fabrication. *Addit. Manuf.* **2020**, *35*, No. 101285.

(30) Barile, C.; Casavola, C.; Cazzato, A. Acoustic Emissions in 3D Printed Parts under Mode I Delamination Test. *Materials* **2018**, *11* (9), 1760.

(31) Pulipaka, A.; Gide, K. M.; Beheshti, A.; Bagheri, Z. S. Effect of 3D printing process parameters on surface and mechanical properties of FFF-printed PEEK. *Journal of Manufacturing Processes* **2023**, *85*, 368–386.

(32) Meredith, J. C.; Sormana, J. L.; Keselowsky, B. G.; García, A. J.; Tona, A.; Karim, A.; Amis, E. J. Combinatorial characterization of cell interactions with polymer surfaces. *J. Biomed Mater. Res. A* **2003**, *66a* (3), 483–490.

(33) Sormana, J. L.; Meredith, J. C. High-throughput discovery of structure-mechanical property relationships for segmented poly(urethane-urea)s. *Macromolecules* **2004**, *37* (6), 2186–2195.

(34) Sormana, J. L.; Chattopadhyay, S.; Meredith, J. C. High-throughput mechanical characterization of free-standing polymer films. *Rev. Sci. Instrum.* **2005**, *76* (6), No. 062214.

(35) Shin, D.; Choi, W. T.; Lin, H.; Qu, Z.; Breedveld, V.; Meredith, J. C. Humidity-tolerant rate-dependent capillary viscous adhesion of bee-collected pollen fluids. *Nat. Commun.* **2019**, *10* (1), 1379.

(36) Lopes, L. R.; Silva, A. F.; Carneiro, O. S. Multi-material 3D printing: The relevance of materials affinity on the boundary interface performance. *Additive Manufacturing* **2018**, *23*, 45–52.

(37) ASTM *D638: Standard Test Method for Tensile Properties of Plastics*; 2010. DOI: .

(38) Zapata, P.; Mountz, D.; Meredith, J. C. High-Throughput Characterization of Novel PVDF/Acrylic Polyelectrolyte Semi-Interpenetrated Network Proton Exchange Membranes. *Macromolecules* **2010**, *43* (18), 7625–7636.

(39) ASTM *E2546-Standard Practice for Instrumented Indentation Testing*; 2015. DOI: .

https://doi.org/10.1021/acsapm.4c00921
ACS Appl. Polym. Mater. 2024, 6, 9430–9439

(40) Wan, K.-t.; Liao, K. Measuring mechanical properties of thin flexible films by a shaft-loaded blister test. *Thin Solid Films* **1999**, *352* (1−2), 167−172.
(41) Brackett, J.; Cauthen, D.; Condon, J.; Smith, T.; Gallego, N.; Kunc, V.; Duty, C. The impact of infill percentage and layer height in small-scale material extrusion on porosity and tensile properties. *Addit. Manuf.* **2022**, *58*, No. 103063.
(42) Duty, C.; Failla, J.; Kim, S.; Smith, T.; Lindahl, J.; Kunc, V. Z-Pinning approach for 3D printing mechanically isotropic materials. *Additive Manufacturing* **2019**, *27*, 175−184.

https://doi.org/10.1021/acsapm.4c00921
ACS Appl. Polym. Mater. 2024, 6, 9430−9439